ENERGETIKA. 2007. T. 53. Nr. 3. P. 62–71

Comparison of axisymmetrical computations of explosion with various 3D-structure models

Marie-France Robbe

38 Rue de Migneaux,
91300 Massy, France
E-mail: sdufour@free.fr

MARS is a small-scale replica of the Fast Breeder Reactor, which contains all the internal structures of the reactor block. In the experiment, the fluids intervening in a real Core Disruptive Accident are replaced by water, argon and an explosive charge. The goal was to investigate the mechanical effects of a Hypothetical Core Disruptive Accident.

Several 2D-axisymmetrical simulations of the MARS test were carried out. As it was not possible to mesh the peripheral 3D-structures of complex geometry, they were accounted for in different ways: no description, pressure loss or porosity model. Some local and temporary differences appear during the explosion according to the model, but the numerical results remain close, except in the vicinity of the porous zone. The numerical results are globally in good agreement with the test.

Key words: nuclear reactor, explosion, fluid-structure coupling, homogenization

1. INTRODUCTION

Based on small-scale models of the Liquid Metal Fast Breeder Reactor, the MARA-MARS programme [1] was performed at the CEA-Cadarache in the 1970–1980s to investigate the mechanical effects of a Hypothetical Core Disruptive Accident (CDA) in a Liquid Metal Fast Breeder Reactor (LMFBR). In case of CDA, the contact between hot fuel and liquid sodium creates in the core a high-pressure gas bubble whose expansion loads and deforms the vessel and the internal structures.

The MARA-MARS programme involved eleven tests of gradual complexity due to the addition of internal deformable structures:

– MARA 1, 2 considered a vessel partially filled with water and closed by a rigid roof [2];

– MARA 3 to 7 represented the presence of internal components added step by step [3];

– MARA 8 and 9 were closed by a flexible vessel and a flexible roof [4];

– MARA 10 included the core support structures and a simplified representation of the structures above the core [5];

– MARS [6] was a 1/20-scale mock-up including all the significant internal components.

Initially, simulations of the MARA tests were performed with the SIRIUS code [7] specialized in the modelling of CDAs. But at the end of the 1980s, it was preferred to develop a specific CDA sodium-bubble-argon tri-component constitutive law [8] in the general ALE fast dynamics finite element CASTEM-PLEXUS code. The first version of the law was validated [9] with the CONT benchmark [10].

In order to demonstrate the CASTEM-PLEXUS capability to predict the behaviour of real reactors [11], axisymmetrical computations of the MARA series were confronted with the experimental results. The computations performed early in the 1990s showed a rather good agreement between the experimental and computed results for the MARA 8 and MARA 10 tests, even if there were some discrepancies [12]. On the contrary, the prediction of the MARS structure displacements and strains was overestimated [13].

In 1999, the CASTEM-PLEXUS code was merged with the PLEXIS-3C code [14] (a former joint product by CEA and JRC) to extend the capacities of both codes. The new-born EUROPLEXUS code benefited from a new method to deal with the fluid-structure coupling.

New simulations were undertaken with the new coupling and compared with the experimental results for the MARA 8 mock-up [15] and the MARA 10 mock-up [16].

Three numerical simulations of the MARS test were carried out:

– a reference simulation [17] with a finer mesh and no description of the peripheral components;

– a description of the non-axisymmetrical peripheral structures (pumps and heat exchangers) by a pressure loss [18] to estimate the influence of the latter structures [19];

– a description of the peripheral structures with a porous model [20] to account for their protective effect on the vessels by absorbing energy and slowing down the fluid impacting the vessels without meshing them.

The paper offers a comparison of the numerical results computed by different methods with the experimental results.

2. THE MARS MOCK-UP

The primary circuit of the French LMFBR reactor (Fig. 1) is enclosed in the main reactor vessel. This vessel is welded to the

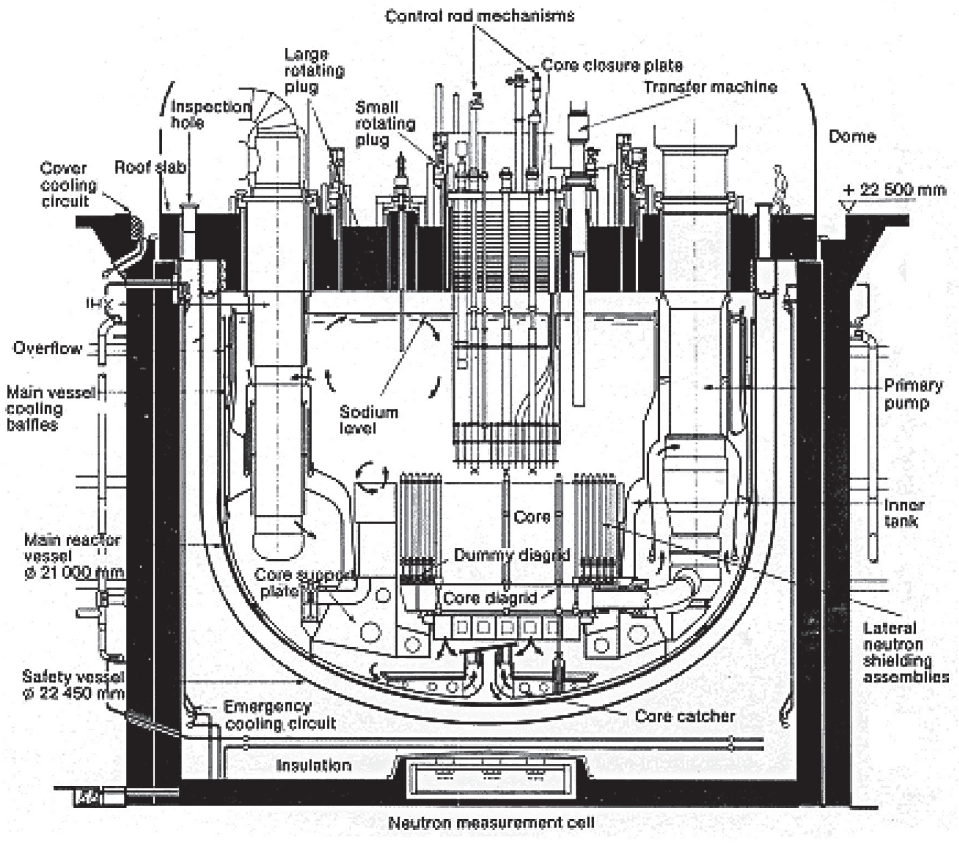

Fig. 1. A liquid metal fast breeder reactor

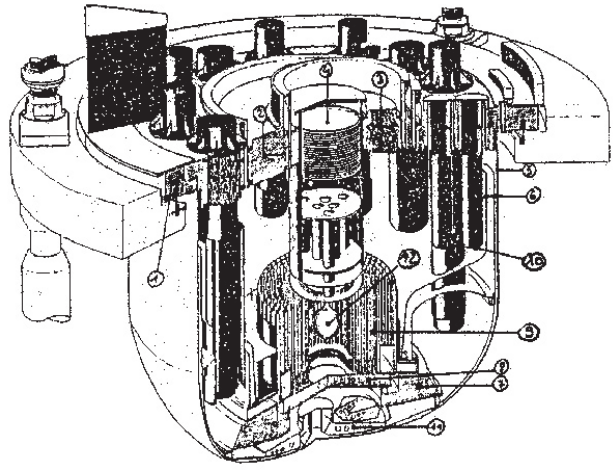

mark 1: roof
mark 2: large rotating plug
mark 3: small rotating plug
mark 4: core cover plug
mark 5: main vessel
mark 6: internal vessels
mark 7: core support structures
mark 8: diagrid support
mark 9: core and neutron shieldings
mark 10: pumps and heat exchangers
mark 11: core catcher
mark 12: core

Fig. 2. The MARS mock-up

roof slab and encased in a safety vessel. Both vessels are made of stainless steel.

The MARS experiment (Fig. 2) is a 1/20-scale mock-up of a LMFBR block. The main vessel (1 m in diameter and 1 m high) includes all the significant internal components of the reactor [6].

The main vessel is an assembly of a cylindrical part made of 316L stainless steel and a torospherical bottom made of 304L stainless steel. Its thickness varies between 0.8 and 1.6 mm.

The unmelted part of the core is simulated by aluminum cylinders and steel hexagons fixed into two AG3 aluminum plates. The neutron shielding is represented by four radial shells and associated supporting structures.

The mock-up also includes the strongback, the diagrid support, two inner vessels, the anti-convecting device, the core catcher and the main vessel cooling system.

The roof slab is constituted by two circular plates of different thickness. Openings are drilled to enable the passage of the large components. The two rotating plugs are concentrically off as in the reactor. The core cover plug was simplified compared to the reactor one; however, it includes a top plate, a heat-insulation, spacer plates, an in-pile shell and pipes.

The main components inserted through the roof slab (4 primary pumps, 8 intermediate heat exchangers, 4 emergency cooling exchangers, 2 integrated purification devices), as well as the supporting and joining rings are present. Rubber-ring bands simulate the heat-insulating material between the roof and the main vessel. The other components above the top closure are represented by their inertia using lead plates.

The thin structures are mainly made of 304L stainless steel in order to simulate the austenistic steel of the reactor structures. The massive structures and those made of heterogeneous materials (roof slab, rotating plugs, core support structure, diagrid support) are made of A5 aluminum. The top plate of the core cover plug is made of A42 aluminum.

The sodium coolant at operating conditions is simulated by water at 20 °C. The cover gas of the mock-up is the same as in the reactor (argon). The test was fired using a 80 g low-density low-pressure explosive charge of L54/16 composition [21]. The charge mass was chosen to simulate the 800 MJ full-scale mechanical

energy release used in the reference CDA in a LMFBR. The explosive charge was supported by the base of the core cover plug.

The test was well instrumented with pressure transducers, accelerometers, strain gauges, high-speed cameras and a grid drawn on the different structures.

3. NUMERICAL MODELING OF THE MOCK-UP

3. 1. Geometry

Owing to the symmetry of the MARS mock-up, a 2D-axisymmetrical representation was chosen. The external structures are modelled by shells or massive elements. The main internal structures are represented by a classical shell model.

The main vessel is modelled with three thin shells of different thickness and two materials for the cylindrical and torospherical parts. The vessel is supposed to be embedded in the roof. The mock-up is fixed to the rigid frame by a cylindrical shell.

The top closure is composed of massive elements and assimilated to an axisymmetrical structure for the needs of the numerical simulation. The openings for the passage of the components (pumps, heat exchangers) are simply accounted for by the mass they remove to the roof. Local masses are added above the top closure to consider the mass of the instrumentation, the lead plates, and the peripheral components.

The core cover plug was simplified. The upper part is modelled by the top plate. Three plates simulate the heat and neutronic insulation. The pipes are assimilated to two cylinders.

The rings joining the roof slab and the three plugs are represented by thin aluminum shells at the top of the massive pieces. Complementary shell elements made of rubber and joining the base of the massive structures were added to prevent the going up of argon in the free slit. The heat-insulating material between the roof base and the main vessel is represented by a rubber-ring band.

In the centre of the mock-up, a single rigid structure (called Core Support Structures) describes the strongback, the neutron shielding support, the support of the baffles and the internal vessel as they are fitted together. The CSS is assimilated to an axisymmetrical rigid shell of constant thickness, whose mass is the total mass of all the structures. The CSS is attached to the vessel by a cylindrical collar.

The diagrid support is described by a thin shell connected to the CSS by a swivel link. The core is schematised by an added mass distributed along the diagrid. The central shell of the neutron shielding is modelled while the three other shells are taken into account by a local added mass located at the base of the central shell.

The baffles surrounding the neutron shielding are assimilated to a vertical axisymmetrical shell. The central shell of the internal vessel is meshed; the second one is described by a local mass. The shielding, the baffle, and the internal vessel are embedded in the CSS. The core catcher is represented by an added mass spread along the bottom of the main vessel.

According to the simulations, the peripheral components (heat exchangers and pumps) are not described, described with a pressure loss, described with the porosity model homogenizing the components with the surrounding fluid. In the porous model, the fluid elements comprised between the extreme radii of the peripheral components are homogenized with the structures. The structures are described by a volume filling rate of 47 \%.

Figure 3 presents the mesh used for simulations with EUROPLEXUS. Figure 4 presents the mesh used with CASTEM-PLEXUS; the size of the cells is much larger. Figures 5 and 6 show the structures for the simulation with the pressure loss and for the simulation with the porosity model, respectively.

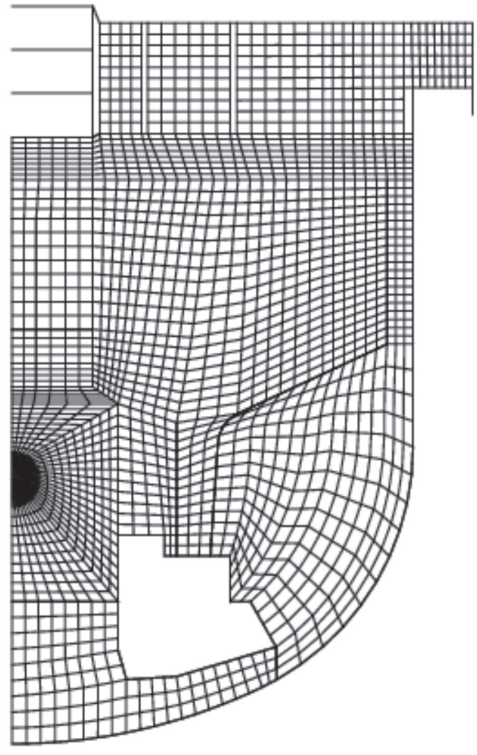

Fig. 3. Mesh of the EUROPLEXUS simulations

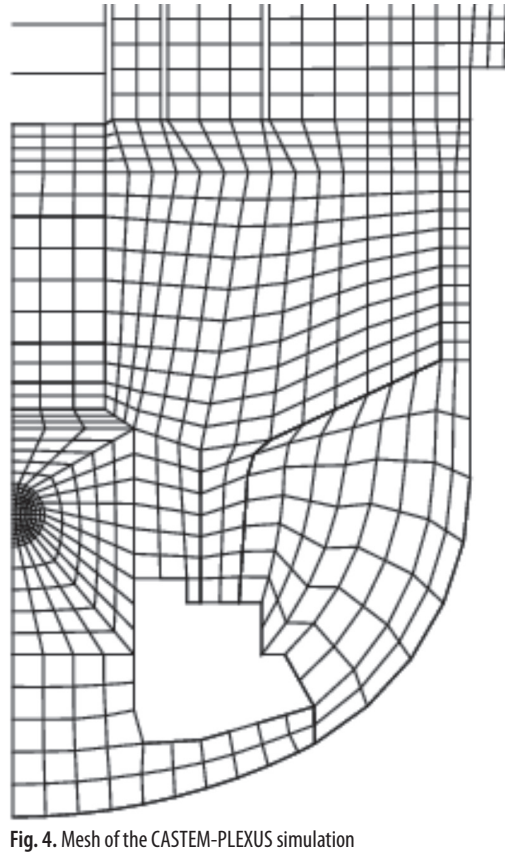

Fig. 4. Mesh of the CASTEM-PLEXUS simulation

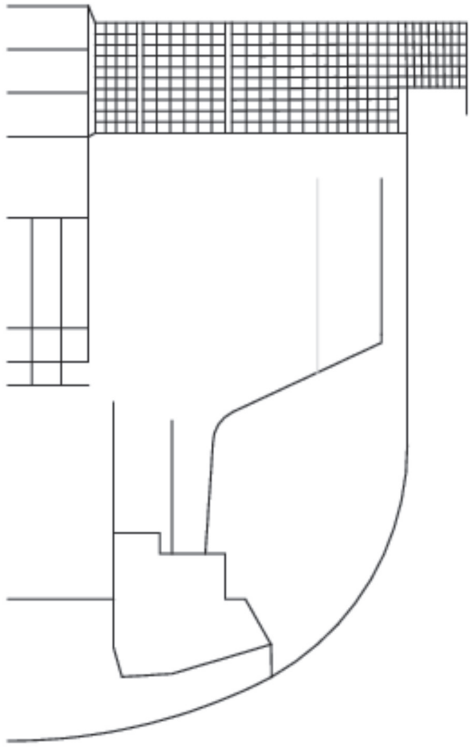

Fig. 5. Mesh of the structures in the pressure loss simulation (the pressure loss is located on the grey line)

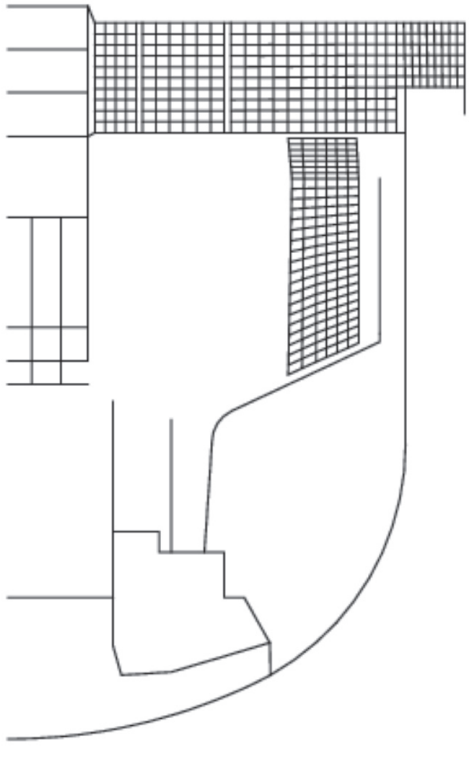

Fig. 6. Mesh of the structures with the porous model (the porous zone is the additional meshed area)

3.2. Materials

The behaviour of the structures is generally described by isotropic elasto-plastic constitutive laws. However, elastic laws are used for the rubber elements of weak resistance, joining the roof and the plugs. The internal and medium cylinders schematizing the pipes of the core cover plug are described by the elastic law approximated by homogenization of non-axisymmetrical structures. The behaviour of the core support structure is supposed to be linear elastic.

The CDA constitutive law is used to describe all the fluid filling the mock-up. This law is devoted to tri-component fluid mixtures for which one of the components can be diphasic. In the mock-up, the fluid intervening are water, argon and the explosive charge.

Argon is supposed to be a perfect gas with an adiabatic behaviour $p_a^{n+1} = p_a^n (\rho_a^{n+1}/\rho_a^n)^{\lambda_a}$ where the initial density $\rho_a^{(o)} = 1.658$ kg/m^3 and the heat capacity ratio $\lambda_a = c_p / c_v = 1.67$. Argon is initially at the atmospheric pressure $p_a^{(0)} = 10^5$ Pa.

The explosive charge (bubble) is described by a perfect gas with a polytropic law $p_b^{(n+1)} = p_b^{(n)} (\rho_b^{(n+1)} / \rho_b^{(n)})^{\Psi_b}$ where the initial density $\rho_b^{(0)} = 400$ kg/m^3, the initial pressure $p_b^{(0)} = 2.88\ 10^8$ Pa and the polytropic coefficient $\Psi_b = 1.322$.

Water is described by a perfect and isothermal fluid $p_w^{(n+1)} = p_g^{(n+1)} = p_w^{(n)} + C_w^2 (\rho_w^{(n+1)} - \rho_w^{(n)})$ with an initial density $\rho_w^{(0)} = 998.3$ kg/m^3, a sound velocity $C_w = 550$ m/s. Water is initially at the atmospheric pressure $p_w^{(0)} = 10^5$ Pa.

The pressure of the gas mixture p_g is the sum of partial pressures of gases: $p_g^{(n+1)} = p_a^{(n+1)} + p_b^{(n+1)} + p_v^{(n+1)}$.

Water is supposed to be in saturation condition. However, if $p_w^{(n+1)} > p_{sat}$, the present fraction of vapour is negligible. If the pressure decreases, water can reach the saturation pressure, and the vaporisation is supposed to be instantaneous. Vapour is an isothermal perfect gas whose pressure is constant and only depends on the initial temperature $T^{(0)}$:

$$p_v^{(n+1)} = p_{sat}(T^{(0)}).$$

3.3. Grid update

In the simulations of the MARS test, structures are represented with a Lagrangian description. The bubble zone is kept fixed and is Eulerian. The water and the argon are described by an ALE modelling (Arbitrary Lagrange Euler): the fluid grid is updated according to the deformation of the neighbouring structures. The porosity model implemented in EUROPLEXUS being available only for the Eulerian description, the homogenized zone must be Eulerian. Two element layers next to the internal vessel are let out of the homogenized zone to operate the fluid–structure coupling.

3. 4. Fluid-structure coupling

The fluid–structure coupling implemented in EUROPLEXUS works without coupling elements. The code automatically writes relations between the fluid and solid nodes facing each other. The fluid can flow tangentially to the structure. This coupling is well adapted to complex geometries, but it requires sometimes a user intervention to pilot the displacements of the fluid ALE grid.

In the CASTEM-PLEXUS computation, the coupling existing at the time required the definition of coupling elements by the user and imposed to the fluid nodes to have the same displacements as the structure nodes. In addition, there was no automatic update of the ALE grid for the elements other than the ones on the coupled lines.

3. 5. Boundary conditions

The boundary conditions are:

– complete blocking of the base of the shell fixing the mock-up to the rigid frame;

– no rotation of all the nodes of the top closure at the intersection between the massive structures and the shells;

– no horizontal displacement and no rotation of the structure and fluid nodes located on the symmetry axis;

– no horizontal displacement of the rigid CSS;

– vertical displacement of the CSS equal to that of the intersection between the collar and the vessel;

– same vertical displacement for the four plates simulating the heat and neutronic insulation of the core cover plug.

4. COMPARISON WITH EXPERIMENTAL AND PREVIOUS NUMERICAL RESULTS

The CASTEM-PLEXUS simulation was characterized by a rough mesh, a fluid–structure coupling based on coupling elements, and a description of the peripheral structures with a pressure loss. The EUROPLEXUS simulations use a fine mesh and a new treatment of the fluid–structure coupling. The three EUROPLEXUS simulations differ by the modelling of the peripheral structures: no description, pressure loss model, or porous model.

4. 1. Comparison of the explosive phenomenon

This comparison concerns the two last EUROPLEXUS simulations with the pressure loss model and the porous model. As the results of the EUROPLEXUS simulation without any description of the peripheral components are very close to those of the simulation with the pressure loss, the first simulation is not used in the present comparison. In figures, the pressure loss model is presented on the left side and the porous model on the right side.

The presence of the peripheral porous structures introduces some local perturbations in the propagation of the pressure shock wave inside the porous zone and in the vicinity (Figs. 7 and 8). When the shock wave crosses the porous zone at 0.34 ms, pressure increases at the entrance of the porous zone and a kind of checker-board appears in the layers between the inner vessel and the porous zone. Part of the shock wave is reflected backwards in the porous model at 0.38 ms, as the interface behaves as a porous wall. This effect comes from the interaction force

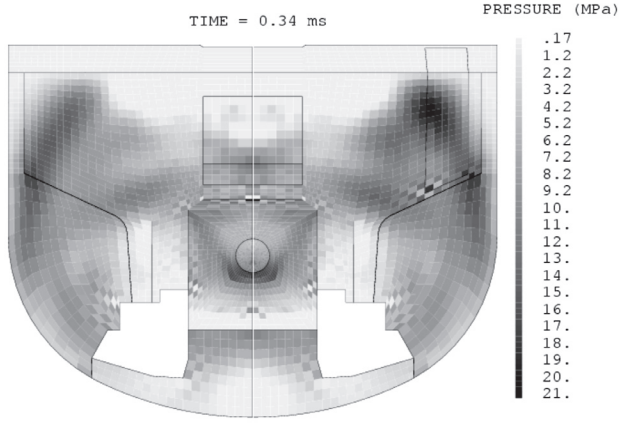

Fig. 7. Pressure at 0.34 ms

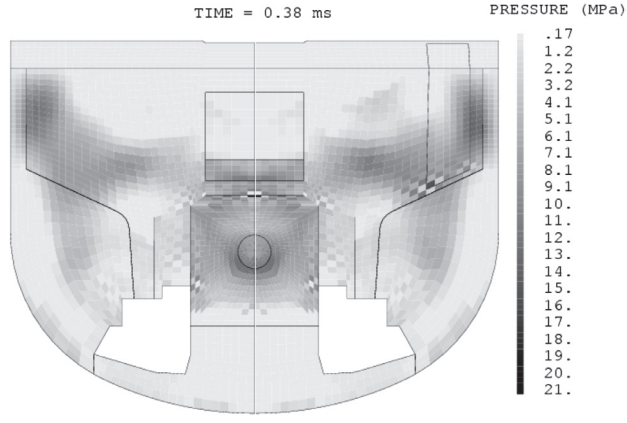

Fig. 8. Pressure at 0.38 ms

$\vec{F}_{eq}$ at the interface. Afterwards, pressure decreases in the whole mock-up in both simulations.

The vaporisation of water is much higher in the porous zone between 1 and 3 ms (Fig. 9). As the density is proportional to the porosity, it appears lower in the porous zone. When the fluid is in saturation conditions, the lower density corresponds to a higher rate of vapour.

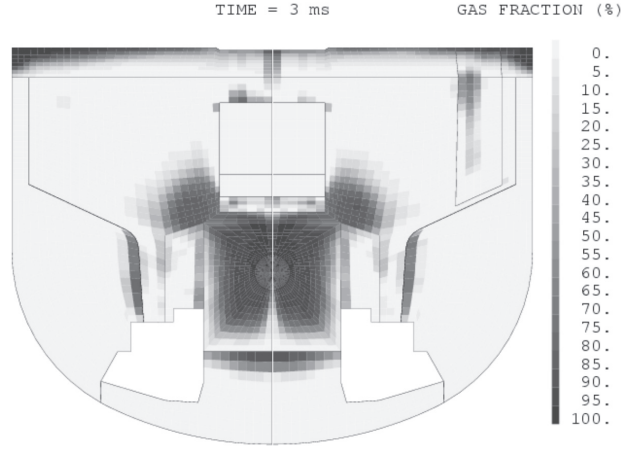

Fig. 9. Gas fraction at 3 ms

It is possible to observe from 2 ms that the porous zone forms an obstacle that deviates the flows upwards and accelerates argon flows along the top closure (Fig. 10). The impact of argon on the top right-hand corner of the mock-up and the downward massive flows in the channel between the inner vessel and the main vessel happen sooner in the porous model.

The top of the main vessel starts deforming at 5 ms in the porous model and a bit later in the pressure loss model. The Above Core Structures are more lifted in the pressure loss model than in the porous model (Fig. 11).

The bubble panache expands less in the upper zone between 8 and 10 ms as the presence of the porous zone limits the volume available for the expansion. In the porous model, part of the water flows is deviated upwards along the porous zone and then inwards near the top closure. Simultaneously, argon flows very fast over the porous zone. These contradictory flows create waves below the top closure, and the argon layer is stretched down in the porous model (Fig. 12).

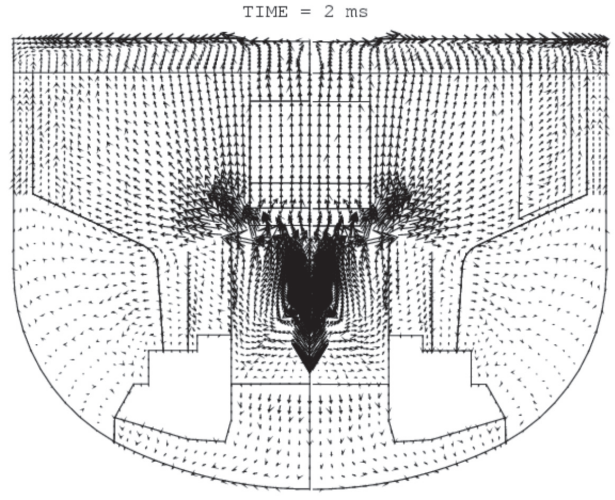

Fig. 10. Fluid flows at 2 ms

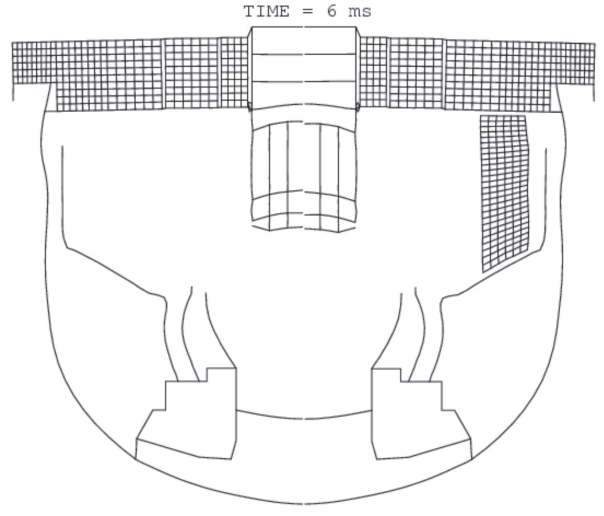

Fig. 11. Deformed mesh at 6 ms

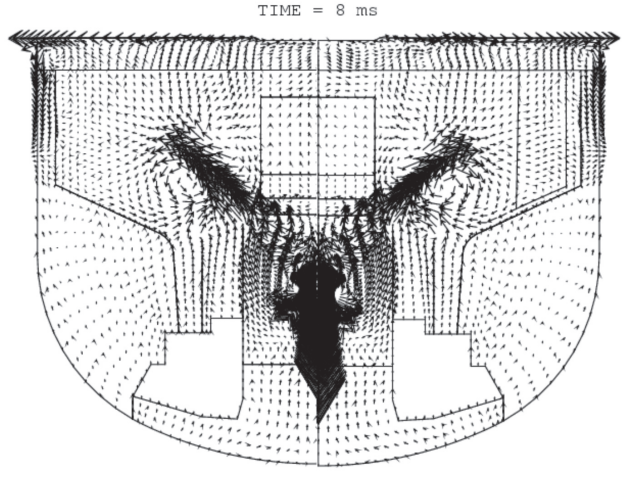

Fig. 12. Fluid flows at 8 ms

The main whirlpool formed in the upper zone rotates in a more narrow space in the porous model, thus it propels more violently the fluid in the central zone, and the small whirlpool in the central zone is more intense (Fig. 13).

Globally, the explosive phenomenon is similar in both simulations with the pressure loss and the porous model. The deformed shape at the end is very close (Fig. 14). Some local and temporary differences appear during the explosion, but they do not induce major changes in the final results.

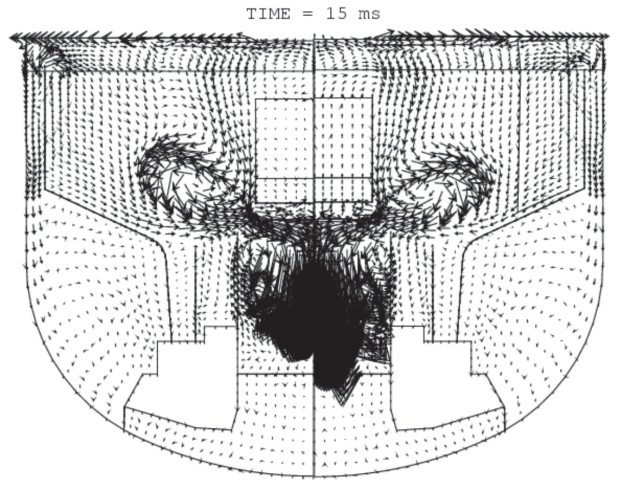

Fig. 13. Fluid flows at 15 ms

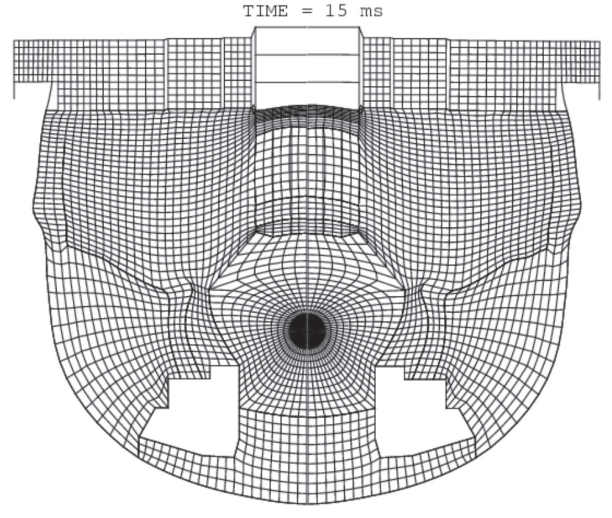

Fig. 14. Deformed mesh at 15 ms

4. 2. Comparison of the structure deformations

The comparison concerns:

– the vertical displacement of the main vessel base, the roof, the diagrid support, and the in-pile shell;

– the radial displacement of the top of the lateral neutron shielding, the top of the baffle, the main vessel at the junction with the collar, the internal vessel at the top of the lower part and at the bulge level in the upper part;

– the hoop strain of the vessel upper bulge;

– the maximum impact pressure under the large rotating plug and the roof.

In the figures, the simulation with the porous model corresponds to the bold lines, while the simulation with the pressure loss is presented by thin lines. Table presents a synthesis of all the results: experiment, CASTEM-PLEXUS simulation (noted CP), EUROPLEXUS simulation without the peripheral structures (noted EP1), EUROPLEXUS simulation with the pressure loss model (noted EP2), and EUROPLEXUS simulation with the porous model (noted EP3).

Table. **Comparison of experimental and numerical results**

		Experiment		CP		EP1		EP2		EP3	
		Max	Final	Max	Final	Max	Final	Max	Final	Max	Final
Main vessel bottom	Vertical displacement (mm)	–14	–9	–34	–26	–21	–12	–21	–12	–21	–12
Junction main vessel – collar	Vertical displacement (mm)	–6		–10		–10	–1.5	–10	–1.5	–10.5	–2
Main vessel upper bulge	Hoop strain (%)	2.4	1.9	4.8	4.4	5.2	4.9	4.4	4.2	4.9	4.6
Roof	Vertical displacement (mm)	5.5	5	12	5	11	3.8	11	3.8	11.1	3.9
Diagrid support	Vertical displacement (mm)		–18		–23	–31	–20.5	–31	–20.5	–31	–20.5
CCP in-pile shell	Vertical displacement (mm)		97	70	70	100	83	102	86	99	86
Neutron shielding	Radial displacement (mm)	54	50		53	64	63	64	62.5	63	62
Baffle	Radial displacement (mm)		15		14	25	22.5	25.5	22	24	21
Internal vessel	Radial displacement (mm) at the top of the lower part	19	15		10	18.5	13.7	18.5	14	18	13.8
	Radial displacement (mm) of the bulge in the upper part		10		15	12.2	11.3	11.5	10.5	15	14.2
Pressure under the large rotating plug	Max. pressure (MPa)	19.4		3.6		5.3		5.7		3.2	
	Instant of maximum (ms)	3		3		4		4		3.5	
Pressure under the roof in the argon	Max. pressure (MPa)	5.4		2		3.3		3.4		3.3	
	Instant of maximum (ms)	4.1		7		3.5		3.8		4.3	

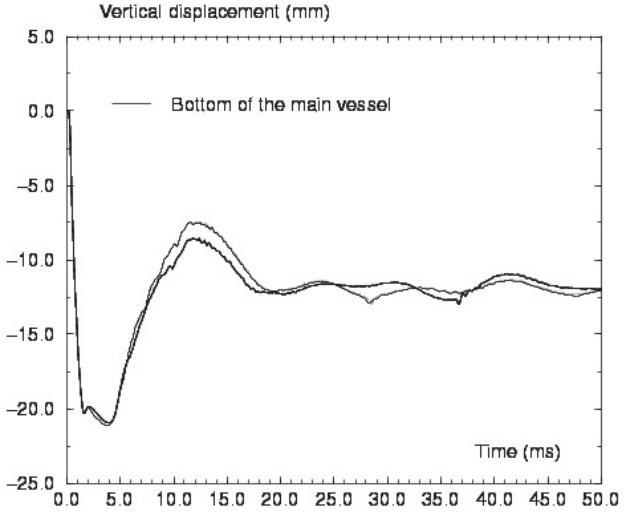

Fig. 15. Vertical displacement at the bottom of the main vessel

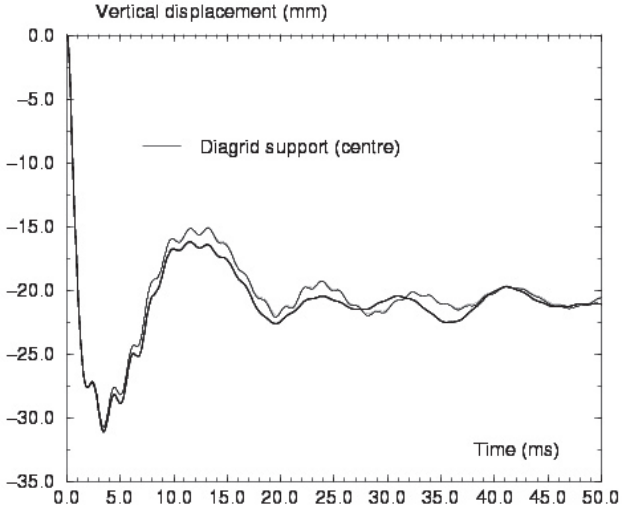

Fig. 16. Vertical displacement of the diagrid support

Figures 15 and 16 present vertical displacements of the main vessel bottom, the diagrid support.

Regarding the behaviour of the main vessel at the bottom, the three EUROPLEXUS computations are very close. If the results are better than those of CASTEM-PLEXUS, they present an error of 50% for the maximum value and 22% at the end, compared with the experimental values. At the junction with the collar, the displacements present an error of 66%.

Concerning the upper bulge, Fig. 17 displays the points where the evolution of the displacement versus time is recorded in the new EUROPLEXUS computation. The comparison with the experimental data concerns the area of point 3. The simulation with the porous model is the least precise, with an error higher than 100% in relation to the experiment.

This lack of accuracy may come from the modelling of the porous zone. As the porous model is only available in Eulerian description, it is necessary to let two rows of ALE elements between the porous zone and the shells. The rows near the top closure induce accelerated flows along the top closure; when propa-

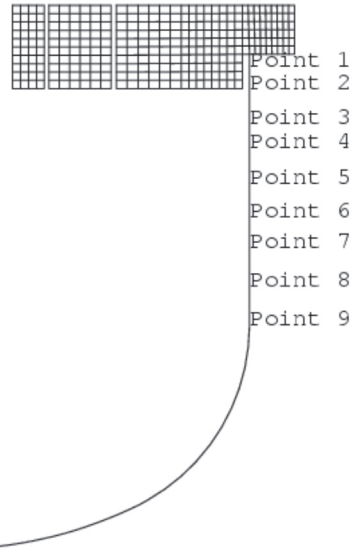

Fig. 17. Location of the points used to describe the main vessel upper bulge

gating into the channel, these more intense flows deform more the main vessel.

With the porous simulation, the maximum radial displacement is recorded for points 5 and 6, just above the bottom of the channel. The upper bulge forms at the top and then lowers, following the downward flows in the channel between both vessels. In the CASTEM-PLEXUS simulation, the upper bulge happened at the level of point 4: in the absence of several element layers in the channel, the old coupling did not allow large fluid flows in the channel.

As regards the vertical displacement of the top closure, the maximum value is computed in the CCP: 29 mm in the centre. The displacement is a bit lower in the small rotating plug (around 17–18 mm) and in the large rotating plug (between 14 and 16 mm). In the roof, the maximum displacement concerns the junction with the large rotating plug and is around 11 mm. At a mid-distance between the plug junction and the main vessel, the displacement reaches a maximum of 7 mm, whereas near the vessel the maximum value is no more than 3.5 mm. The values noted in the different components confirm the deformation in stairs of the top closure with a vertical gap of some millimetres between two massive components.

We suppose that the comparison relative to the vertical displacement of the roof concerns the top left corner of the roof, near the rotating plug. All the EUROPLEXUS results are very close. The prediction of the maximum displacement remains far from the experimental result (100 % error), whereas the final displacement fits well with the test (22% error).

Concerning the diagrid support displacement, we note a maximum displacement of 31 mm at 3.5 ms and a final displacement of about 21 mm at 50 ms. Once again, the EUROPLEXUS and CASTEM-PLEXUS are very close. The prediction of the final displacement is in good agreement with the experiment (17% gap).

The comparison relative to the CCP in-pile shell fits well with the experiment, even if the EUROPLEXUS computations underestimate the vertical displacement of 13%. The EUROPLEXUS results are very close and more precise than that computed by CASTEM-PLEXUS. The reason for this improvement comes from the mesh fineness, which is twice the one of the CASTEM-PLEXUS computation. Consequently, in the EUROPLEXUS simulations, the CCP shells seem much more flexible. The buckling of the external cylinder is more marked and thus the vertical displacement of the whole core cover plug is increased.

The radial displacement of the top of the lateral neutron shielding computed by EUROPLEXUS is relatively precise, even if the simulations overestimate by 17% the maximum displacement and by 24% the final one. The EUROPLEXUS computations are similar and less precise than the CASTEM-PLEXUS one. The overprediction may come from the fact that only the central one of the four lines of the neutron shielding is modelled in the simulations and thus this single shell is less rigid than the set of four shells.

Concerning the radial displacement of the baffle, the last simulation shows an error of 28%. It is difficult to compare the EUROPLEXUS and CASTEM-PLEXUS results: in the CASTEM-PLEXUS simulation, the baffle was completely blocked from the base to mid-height, while in the EUROPLEXUS simulations the baffle can move freely. Considering this condition, it is normal to observe a larger displacement in the EUROPLEXUS simulations.

Regarding the radial displacements at the top of the lower part of the internal vessel, the simulations fit almost exactly with the test, both for the maximum (5% error) and final values (8% error).

The prediction of the bulge appearing in the upper part of the internal vessel is very precise for the EUROPLEXUS simulations without the peripheral structures, and with the pressure loss model. The simulation with the porous model is much less precise (42% error). As for the upper bulge in the main vessel, it seems that the rows of ALE elements surrounding the porous zone induce large flows that lead to an excessive deformation of both vessels.

As for the pressure peaks observed under the top closure, all the simulations predict the peaks at the right time, but the amplitude of the peaks is largely underestimated.

In the simulation by the pressure loss model, we can observe a high pressure peak up to 8 MPa in the corner formed by the roof and the main vessel. This value is approximately twice the average pressure elsewhere under the top closure and is due to the rebound of the shock wave against the wall.

Globally, the EUROPLEXUS results at the end of the computations are in good agreement with the test, except for the upper bulges of the main and internal vessels.

The results concerning the maximum displacements are less precise for the main vessel and the roof. The pressure peaks under the roof are predicted at the right time, but the amplitude of the peaks is really underestimated.

The three EUROPLEXUS simulations provide very close results, except the simulation with the porous model in the vicinity of the porous zone. Globally, the EUROPLEXUS simulations overestimate the displacements of the structures, apart from that of the in-pile shell. The displacements of the central structures (CCP in-pile shell, neutron shielding, baffle, the lower part of the internal vessel) are higher with the EUROPLEXUS models than with the CASTEM-PLEXUS model. These extra-displacements come from both the mesh refining (the finely meshed structures seem to be more flexible than those of the rough mesh) and the new coupling that allows tangential fluid flows along the shells.

5. CONCLUSIONS

This paper presents a comparison of computed and experimental results concerning explosion in the MARS mock-up. MARS is a small-scale replica of the Fast Breeder Reactor which contains all the internal structures of the reactor block. The fluids intervening in a real Core Disruptive Accident are replaced by water, argon and an explosive charge in the experiment.

In the numerical model, the majority of the structures are represented by axisymmetrical shells or massive structure. As it is not possible to mesh the peripheral 3D-structures of complex geometry, they are taken into account in different ways. The internal fluids are described by the specific CDA constitutive law implemented in the EUROPLEXUS code to describe transients involving diphasic inviscid tri-component mixtures.

Four simulations of the MARS test were carried out up to now with the CASTEM-PLEXUS code in 1995 and with the EUROPLEXUS code from 2000 (after the merging of the CASTEM-PLEXUS code with the PLEXIS-3C code). The CASTEM-PLEXUS

simulation was characterized by a rough mesh, a fluid–structure interaction based on coupling elements and the representation of the peripheral components by a pressure loss.

The EUROPLEXUS simulations use a finer mesh and a fluid–structure interaction allowing tangential flows along structures. The reference simulation with no description of the peripheral components and the simulation with a pressure loss to describe the non-axisymmetrical peripheral structures show very close results. With the porous model, the explosive phenomenon is globally similar to both previous simulations and the final deformed shape is very close. Some local and temporary differences appear during the explosion, but they do not induce major changes in the results.

The presence of the peripheral porous structures introduces local perturbations in the propagation of the pressure shock wave. The porous zone deviates the flows upwards from 2 ms and accelerates argon flows along the top closure. Water vaporises more in the porous zone between 1 and 3 ms.

The impact of argon on the top right-hand corner, the downward massive flows in the channel between the inner vessel and the main vessel, and the formation of the upper bulge in the main vessel happen 0.5 ms sooner in the porous model. The bubble panache and then the main whirlpool have less space available to expand and rotate. Therefore the whirlpool propels fluid more violently in the central zone, and the second whirlpool in the central zone is more intense.

A comparison of the four computations with the experimental results shows that the numerical results at the end of the computations are in good agreement with the test, except for the upper bulges of the main vessel and the internal vessel. The pressure peaks under the roof are predicted at the right time, but the amplitude of the peaks is underestimated.

The three EUROPLEXUS simulations provide very close results, except in the vicinity of the porous zone. Globally, the EUROPLEXUS simulations overestimate the displacements of the structures, apart from that of the in-pile shell.

In the future, improvements of the EUROPLEXUS code should concern development of a porous model for the ALE description. This extension of the model would allow to represent the effect of the central core structures and to extend the porous zone of the peripheral structures up to the near structures (internal vessel and roof).

It would be also useful to reduce again the size of the mesh to be able to represent the four shells of the neutron shielding and the two internal vessels. On the one hand, the presence of these additional shells in the mesh, as well as the core assemblies, should absorb part of the energy of the shock wave and reduce the velocity of flows. On the other hand, the higher rigidity of the four shells of the neutron shielding should deviate the central flows upwards and lift the in-pile shell of the Core Cover Plug.

The description of the additional structures should reduce the underestimation of the displacement of the in-pile shell and the overestimation of the displacements of the other structures. The extension of the porous zone of the peripheral structures should avoid side-effects at the vorder with the near structures.

Received 10 May 2007
Accepted 20 August 2007

References

1. Louvet J. Containment response to a core energy release. Main experimental and theorical issues – Future trends // Proc. 10th Int. Conf. on Structural Mechanics in Reactor Integrity. Anaheim, USA, 1989. Vol. E. P. 305–310.
2. Acker D., Benuzzi A., Yerkess A., Louvet J. MARA 01/02 – Experimental validation of the SEURBNUK and SIRIUS containment codes // Proc. 6th Int. Conf. on Structural Mechanics in Reactor Technology. Paris, France, 1981. Paper E 3/6.
3. Smith B. L., Fiche C., Louvet J., Zucchini A. A code comparison exercise based on the LMFBR containment experiment MARA-04 // Proc. 8th Int. Conf. on Structural Mechanics in Reactor Technology. Brussels, Belgium, 1985. Paper E 4/7. P. 151–157.
4. Fiche C., Louvet J., Smith B. L., Zucchini A. Theoretical experimental study of flexible roof effects in an HCDA's simulation // Proc. 8th Int. Conf. on Structural Integrity in Reactor Technology. Brussels, Belgium, 1985. Paper E 4/5. P. 139–144.
5. Louvet J., Hamon P., Smith B. L., Zucchini A. MARA 10: an integral model experiment in support of LMFBR containment analysis // Proc. 9th Int. Conf. on Structural Mechanics in Reactor Integrity. Lausanne, Switzerland, 1987. Vol. E. P. 331–337.
6. Falgayrettes M., Fiche C., Granet P., Hamon P., Barrau P., Magnon B., Jalouneix J., Nédélec M. Response of a 1/20 scale mock-up of the Superphenix breeder reactor to an HCDA loading simulation // Proc. 7th Int. Conf. on Structural Mechanics in Reactor Technology, Chicago, USA, 1983. Paper E 4/1. P. 157–166.
7. Blanchet Y., Obry P., Louvet J. Treatment of fluid-structure interaction with the SIRIUS computer code // Proc. 6th Int. Conf. on Structural Mechanics in Reactor Technology. Paris, France, 1981. Paper B 8/8.
8. Lepareux M., Bung H., Combescure A., Aguilar J. Analysis of a CDA in a LMFBR with a multiphasic and multicomponent behaviour law // Proc. 11th Int. Conf. on Structural Mechanics in Reactor Integrity. Tokyo, Japan. 1991. Paper E 13/1. P. 371–376.
9. Casadei F., Daneri A., Toselli G. Use of PLEXUS as a LMFBR primary containment code for the CONT benchmark problem. Proc. 10th Int. Conf. on Structural Mechanics in Reactor Technology. Anaheim, USA, 1989. Paper E 13/1. P. 299–304.
10. Benuzzi A. Comparison of different LMFBR primary containment codes applied to a benchmark problem // Nuclear Engineering and Design. 1987. Vol. 100. P. 239–249.
11. Lepareux M., Bung H., Combescure A., Aguilar J., Flobert J. F. 1993. Analysis of an HCDA in a fast reactor with a multiphase and multicomponent behavior law // Proc. 12th Int. Conf. on Structural Mechanics in Reactor Integrity. Stuttgart, Germany, 1993. Paper E 7/2, 197–202.
12. Cariou Y., Spérandio M., Lepareux M., Christodoulou K. LMFBR's whole core accident. Validation of the PLEXUS

code by comparison with MARA tests // Proc. 12th Int. Conf. on Structural Mechanics in Reactor Technology. Stuttgart, Germany, 1993. Paper E 7/4.
13. Cariou Y., Lepareux M., Noé H., LMR's whole core accident. Validation of the PLEXUS code by comparison with MARS test. Proc. 14th Int. Conf. on Structural Mechanics in Reactor Technology. Lyon, France, 1997. Paper P 2/6. P. 339–346.
14. Casadei F., Halleux J. P., Huerta A. Dynamic response of fluid-structure systems by PLEXIS-3C // Proc. European Conf. on New Advances in Computational Structural Mechanics. Giens, France, 1991.
15. Robbe M. F., Lepareux M., Cariou Y. Numerical interpretation of the MARA 8 experiment simulating a Hypothetical Core Disruptive Accident. Nuclear Engineering and Design. 2003. Vol. 220. P. 119–158.
16. Robbe M. F., Casadei F. Comparison of various models for the simulation of a Core Disruptive Accident in the MARA 10 mock-up // Nuclear Engineering and Design. 2004. Vol. 232. P. 301–326.
17. Robbe M. F., Lepareux M., Seinturier E. Computation of a Core Disruptive Accident in the MARS mock-up // Nuclear Engineering and Design. 2005a. Vol. 235. P. 1403–1440.
18. Idel'Cik I. E. Memento des pertes de charge. Coefficients de pertes de charge singulières et de pertes de charge par frottement // Collection de la Direction des Etudes et Recherche d'EDF, Eyrolles, Paris, France, 1986. P. 362.
19. Robbe M. F., Lepareux M., Treille E., Cariou Y. Numerical simulation of an explosion in a small-scale replica of a Fast Breeder Reactor // Journal of Computer Assisted Mechanics and Engineering Sciences. 2005b. Vol. 12. P. 87–116.
20. Robbe M. F., Bliard F. A porosity method to describe the influence of internal structures on a fluid flow in case of fast dynamics problems // Nuclear Engineering and Design. 2002. Vol. 215. P. 217–242.
21. David F. Etude d'une composition explosive flegmatisée. Applications à la déformation d'une cuve // Proc. Symposium sur les hautes pressions dynamiques. Paris, France, 1978.

Marie-France Robbe

AŠINIO-SIMETRINIO SPROGIMO SKAIČIAVIMO, REMIANTIS TRIMATĖS STRUKTŪROS MODELIU, PALYGINIMAS

S a n t r a u k a

MARS – maža greitųjų neutronų reaktoriaus kopija, kuriai būdingos visos šio tipo reaktoriaus vidinės struktūros. Eksperimente darbo agentai, dalyvaujantys aktyviosios zonos pažeidimo avarijoje, yra pakeičiami vandeniu, argonu ar sprogstamąja įkrova. Tyrimo tikslas – mechaninių poveikių nustatymas hipotetinės aktyviosios zonos pažeidimo avarijos atveju.

Tyrime buvo atlikti keli MARS (2D) dvimatės ašinės simetrijos modeliavimai. Kadangi buvo neįmanoma suskaidyti sudėtingos geometrijos trimates (3D) periferines struktūras, jos įvertintos skirtingais būdais: jų visai nemodeliuojant, naudojant slėgio praradimo ar poringumo modelį. Sprogimo metu, priklausomai nuo naudojamo modelio, pasireiškia kai kurie vietiniai ir laikini skirtumai, tačiau skaitiniai rezultatai išlieka panašūs, išskyrus porėtąją zoną. Globaliniai skaitiniai tyrimo rezultatai gerai atitinka eksperimentą.

Raktažodžiai: branduolinis reaktorius, sprogimas, homogenizavimas

Марие-Франце Роббе

СОПОСТАВЛЕНИЕ ОСЕСИММЕТРИЧНЫХ РАСЧЕТОВ ВЗРЫВА С ПРИМЕНЕНИЕМ ТРЕХМЕРНЫХ СТРУКТУРНЫХ МОДЕЛЕЙ

Р е з ю м е

MARS – это копия ядерного реактора на быстрых нейтронах, для которой характерны все элементы внутренней структуры для реактора этого типа. В эксперименте рабочие агенты, участвующие в аварии повреждения активной зоны, заменяются водой, аргоном или взрывчатым зарядом. Цель исследования – определение механических воздействий в случае гипотетической аварии с повреждением активной зоны.

Сложные трехмерные (3D) периферийные структуры оценивались различными способами – они совсем не моделировались при использовании моделей потери давления или пористости. В случае взрыва, в зависимости от используемой модели, проявляются некоторые местные и временные различия, но численные результаты остаются одинаковыми, за исключением пористой зоны. В целом результаты весьма хорошо соответствуют эксперименту.

Ключевые слова: ядерный реактор, взрыв, гомогенизация